Contrib Mineral Petrol (2011) 162:675–689
DOI 10.1007/s00410-011-0618-3

ORIGINAL PAPER

Influence of subsolidus processes on the chromium number in spinel in ultramafic rocks

Martin Voigt · Anette von der Handt

Received: 9 September 2010 / Accepted: 17 February 2011 / Published online: 5 March 2011

Abstract The chromium number of spinel $Cr\#^{sp}$ (atomic ratio of Cr/(Cr+Al)) is an important geochemical parameter for the estimation of the degree of partial melting, temperatures, and provenance in peridotites. In this study, a model has been developed in order to determine the effect of subsolidus reactions on the $Cr\#^{sp}$ in ultramafic rocks. The final model includes temperature-dependent distribution coefficients of relevant reactions as well as solubility data and has been applied to lithologies common in mid-ocean ridge settings. Significant changes in the $Cr\#^{sp}$ are predicted from the application of this model during cooling from 1300 to 800°C at mantle pressures. For spinel lherzolites and harzburgites, the $Cr\#^{sp}$ is predicted to decrease proportional to the absolute values of the $Cr\#^{sp}$ at (constantly) increasing spinel mass. Cpx-dunites show the same trend, although to a lower extent. Websterites show a different behavior with a slight increase in the $Cr\#^{sp}$ due to their lack of olivine. Modal abundance of spinel correlates with the magnitude in $Cr\#^{sp}$ change, too. Finally, these results were tested for possible effects on the calculated degree of partial melting as function of the $Cr\#^{sp}$. Application of the $Cr\#^{sp}$ from a peridotite equilibrated down to 800°C would result in an underestimation of only 1.5 % in the degree of melting, justifying the use of $Cr\#^{sp}$ for estimations of this parameter.

Communicated by J. Hoefs.

M. Voigt (✉) · A. von der Handt
Institut für Geowissenschaften, Mineralogie - Geochemie
Albert-Ludwigs-Universität, Albertstr. 23b,
79104 Freiburg, Germany
e-mail: Martin.Voigt@saturn.uni-freiburg.de

Keywords Chromium number · Spinel · Ultramafic rocks · Partial melting · Mid-ocean ridges

Introduction

Mantle melting

The generation of oceanic crust through partial melting of mantle peridotite is an important process in the evolution of the Earth. Although many studies have focused on mantle melting, occurring by decompression during mantle upwelling, some aspects are still poorly understood. Obvious regional differences in mantle melting and subsequent magma differentiation (e.g. Klein and Langmuir 1987), temporal variations in temperature (e.g. Cipriani et al. 2009), occurrence of domains depleted in ancient melting events (e.g. Harvey et al. 2006; e.g. Liu et al. 2008) are examples that advance our understanding of the complexities of the system Earth. The thorough study of the residues of mantle melting, abyssal peridotites, is therefore crucial to gain a better understanding of these processes.

Spinel peridotites

The mineralogy of peridotites shows various amounts of olivine (ol), orthopyroxene (opx), and clinopyroxene (cpx) and smaller amounts of an aluminous mineral. Depending on pressure, this can be either spinel (sp), garnet or plagioclase. Spinel peridotites are the most common lithology when considering suboceanic upper mantle rocks (Dick 1989). Extraction of mid-ocean ridge basalts (MORBs) during partial melting results in distinctive mineralogical and compositional changes (e.g. Kinzler and Grove 1992)

and provides the base for quantitative models of the processes occurring at depth. Abyssal peridotites, mantle xenoliths, and alpine-type peridotites provide evidence of the mantle below the oceanic crust. The latter are associated with ophiolite sequences exposed at the Earths surface due to orogenic processes and may have been affected by processes related to their obduction. Mantle xenoliths are found enclosed in alkaline basalts and are thought to be carried relatively fast to the Earth surface. Therefore, they often retain the equilibrium composition existing at mantle temperatures and pressures. Abyssal peridotites are exposed at fracture zones associated with mid-ocean ridges (Dick 1989) and along slow to ultraslow-spreading mid-ocean ridges (Dick et al. 2003). Variable uplift rates along the global system of mid-ocean ridges may result in varied cooling histories and thus temperatures of equilibration.

The chromium number in spinel

The degree of partial melting (F) is a fundamental parameter for magma generation. Depending on this parameter, magmas of different composition can be generated from a homogeneous mantle source, represented by the depleted MORB mantel (DMM). Because of the different compatibility of elements in melt and rock, they are either partitioned into the minerals or the melt during partial melting. The strong correlation between modal mineralogy and mineral composition can be used to draw conclusions about the degree of partial melting (Dick et al. 1984; Johnson et al. 1990).

Chromian spinel is a common accessory phase in peridotites and basalts. The spinel structure can accommodate a wide range of di-, tri- and quadrivalent cations of which many can also fit in both (octahedral and tetrahedral) sites (O'Neill and Navrotsky 1984). This results in a wide range of solid solutions exhibited by the spinel group, making them a useful petrogenetic monitor for various processes affecting peridotites (Allan et al. 1988; Dick and Bullen 1984; Hellebrand et al. 2001; Irvine 1965; Sack 1982). The wide range in spinel compositions from massif and abyssal peridotites is thought to reflect variations in the degree of partial melting (Dick and Bullen 1984). Through this, spinel composition is also useful to discriminate between different tectonic settings (e.g., Barnes and Roeder 2001; Dick and Bullen 1984).

The chromium number in spinel $Cr\#^{sp}$ (atomic ratio of Cr/(Cr+Al) in spinel) has long been known to be such an useful petrogenetic indicator (Dick and Bullen 1984). Chromium behaves as a compatible element in spinel, whereas Al strongly partitions into the melt (Jaques and Green 1980). This leads to an increase in the spinel $Cr\#^{sp}$ during partial melting. The $Cr\#^{sp}$ in abyssal peridotites ranges from 0.1 to 0.6 while it extends to higher values in arc settings (Dick and Bullen 1984). Assuming uniform mantle composition prior to the melt extraction event, the $Cr\#^{sp}$ can be used to quantitatively determine the degree of partial melting in the spinel facies field. Hellebrand et al. (2001) empirically determined $F = 10\ln(Cr\#^{sp}) + 24$ based on the correlation between $Cr\#^{sp}$ and trace element concentrations in abyssal peridotites. Although this method underestimates F for highly refractory peridotites, it is often the only quantitative and readily applicable method available in highly serpentinized peridotites. The commonly high degree of serpentinization of abyssal peridotites (e.g. Dick et al. 1984; e.g. Michael and Bonatti 1985) leads to the frequent use of the $Cr\#^{sp}$ method when investigating heavily altered abyssal peridotites because of the alteration resistance of spinel relative to associated silicate minerals.

Subsolidus processes affecting element distribution

After the melt extraction event, residual peridotites are affected by subsolidus processes during cooling and pressure change (Brey and Köhler 1990; Hellebrand et al. 2005; Witt-Eickschen and O'Neill 2005). Although diffusive reequilibration between silicates and spinel at different temperature (T) and pressure (P) conditions ceases when solid-state diffusion becomes increasingly ineffective at low temperatures, several metamorphic reactions can be observed. Whereas ion-exchange reactions between minerals only change the chemical composition of minerals, net-transfer reactions resulting in a shifted modal mineralogy are also possible. Hence, near-solidus compositional information may not be preserved but distorted to either higher or lower values. Zoned pyroxene minerals in contact with spinel in abyssal peridotites have been observed in mantle peridotites (Coogan et al. 2007; Seyler et al. 2007), and the possibility of distortion of the $Cr\#^{sp}$ by cooling has been noted (Coogan et al. 2007). Literature compilations also indicate broad variations on plots between $Mg\#^{ol}$ (atomic ratio of Mg/(Mg+Fe) in ol) and $Cr\#^{sp}$, both considered to be robust melting indices (Ionov et al. 2005).

In addition to its importance to studies of mantle melting, the correlation of $Cr\#^{sp}$ with $Mg\#$ of spinel and silicates, respectively, is used for discrimination of tectonic settings as well as geothermometry. Because Mg-Fe exchange between silicates and oxides is strongly dependent on $Cr\#^{sp}$ through the reciprocal exchange relationship between $Mg\text{-}Fe^{2+}$ and Cr-Al in spinel (Engi 1983), it is incorporated in the formulation of many geothermometers (e.g. Liermann and Ganguly 2003; e.g. Ozawa 1983), the assumption being that this value remains quasi-constant during cooling.

Hence, it is important to quantitatively evaluate possible effects of cooling on the $Cr\#^{sp}$ in order to separate them from effects of partial melting. This study aims to evaluate

the robustness of the $Cr\#^{sp}$ in subsolidus equilibration processes using a thermodynamic approach. We will focus in the following on compositions and conditions relevant to ultramafic rocks occuring at mid-ocean ridges as their solid-state equilibra are best studied to date. The presence of phases like plagioclase or hydrous phases will have further subsolidus effects on spinel composition that lie beyond the scope of this contribution.

Methods

Thermodynamics of solid solutions

Distribution coefficients

In order to evaluate the implications of subsolidus reactions on compositional parameters like the $Cr\#^{sp}$, it is necessary to examine the thermodynamic relations in the corresponding system.

Since the $Cr\#^{sp}$ is directly dependent on the chromium and aluminum content of spinel, ion-exchange reactions of the form

$$Al^{\alpha} + Cr^{\beta} \rightleftharpoons Cr^{\alpha} + Al^{\beta} \tag{1}$$

between phases α and β should have a large effect on this parameter. The exchange between spinel and opx, formulated with the Mg-endmembers,

$$\underset{sp}{MgAl_2O_4} + \underset{opx}{MgCr_2SiO_6} \rightleftharpoons \underset{sp}{MgCr_2O_4} + \underset{opx}{MgAl_2SiO_6} \tag{2}$$

is an example for this type of reaction. At equilibrium,

$$\mu_{Al}^{\alpha\,0} + \mu_{Cr}^{\beta\,0} - \left(\mu_{Cr}^{\alpha\,0} + \mu_{Al}^{\beta\,0}\right) = RT \ln \frac{a_{Cr}^{\alpha} \cdot a_{Al}^{\beta}}{a_{Al}^{\alpha} \cdot a_{Cr}^{\beta}} \tag{3}$$

where $\mu_A^{p\,0}$ is the chemical potential of the pure phase p with component A, and a_A^p is the activity of component A in phase p (e.g Saxena 1973). Because $\mu_A^{p\,0}$ is only dependent on temperature and pressure, the equilibrium constant

$$K = \frac{a_{Cr}^{\alpha} \cdot a_{Al}^{\beta}}{a_{Al}^{\alpha} \cdot a_{Cr}^{\beta}} \tag{4}$$

is also a function of T and P only. The activities can then be substituted by the product of the mole fractions x_A^p and activity coefficients γ_A^p, which gives

$$K = \underbrace{\frac{x_{Cr}^{\alpha} \cdot x_{Al}^{\beta}}{x_{Al}^{\alpha} \cdot x_{Cr}^{\beta}}}_{K_D} \cdot \frac{\gamma_{Cr}^{\alpha} \cdot \gamma_{Al}^{\beta}}{\gamma_{Al}^{\alpha} \cdot \gamma_{Cr}^{\beta}}, \tag{5}$$

introducing the distribution coefficient K_D. Because γ_A^p is dependent on the mineral compositions, K_D is only a constant independent of composition when an ideal solution, defined by $\gamma_A^p = 1$, is realized. However, especially the spinel solid solution is far from being ideal (Petric and Jacob 1982), and therefore expressions for K_D should be functions of compositional parameters like the $Cr\#^{sp}$.

Because the variations of $\mu_A^{p\,0}$ with changing temperature are small, Eq. (3) suggests that $\ln K_D \propto 1/T$. Pressure dependence arises from changes in partial molar volume, which plays only a minor role when considering reactions of type (1) according to Ganguly (2008). Furthermore, there is no reliable geobarometer for spinel lherzolites (Witt-Eickschen and O'Neill 2005), and therefore the majority of published expressions for K_D in this context do not include a term accounting for pressure changes.

Partition coefficients

If an ion is present only in traces (i.e. <0.001 wt%) in two minerals, the stoichiometric controls of the exchange reaction can be neglected, and the partition coefficient

$$D = \frac{x_A^{\beta}}{x_A^{\alpha}} \tag{6}$$

for partitioning of component A between α and β can be approximated. Both Al and Cr are major or minor elements in some spinel lherzolite minerals and trace elements in others. It is therefore appropriate to use partition coefficients in some cases, but distribution coefficients should be valid in general.

It can be seen from comparison of Eqs. (5) and (6) that when multiplying two partition coefficients of reciprocal exchange, the distribution coefficient is obtained.

General aspects

Assumptions

The distribution of Al and Cr between present minerals is calculated assuming

1. a closed system, i.e. no mass transfer in or out occurs,
2. only compositional changes (including mineral modes) through reactions incorporated into the model take place, and
3. equilibrium of these reactions is maintained at all times.

In natural systems, deviations from these assumptions can occur. Serpentinization is a result of the addition of H_2O to the system, and therefore a closed system is not maintained throughout the P-T-path of most residual

peridotites. However, this process only occurs at shallower levels outside the temperature range of interest (see "Temperatures and pressures"), and relict grains contain valuable information about earlier P-T-X conditions. Aside from this, refertilization of residual peridotites can occur by melt entrapment, melt-rock reaction and veining (Hellebrand et al. 2002; Jean et al. 2010). Therefore, it should be kept in mind that these processes are not included in the calculations of this work

Regarding assumption (2), most reactions with a significant influence on the $Cr\#^{sp}$ have been included in the model in this work. However, there is no reliable expression for the Al solubility in cpx at present. It is assumed that other reactions in spinel lherzolites only have small effects on the $Cr\#^{sp}$ and lead to minor uncertainties.

The assumption of thermodynamic equilibrium is realized in natural samples to variable degrees. Depending largely on cooling rates and diffusion coefficients, non-equilibrium is possible in rapidly cooled peridotites. Compositional mineral zoning is often the result, if diffusion cannot fully compensate this temperature change (e.g. Bodinier et al. 1987; e.g. Nagata et al. 1983). Especially when temperatures near the closing temperature are reached, deviations from equilibrium increase systematically during further cooling (Coogan et al. 2007). The models presented here do not account for these effects, but comparisons to zoned minerals are presented.

Temperatures and pressures

Temperatures of interest are limited by the initiation of partial melting at high temperatures and by the closure temperature as a lower boundary. Robinson et al. (1998) experimentally determined solidus temperatures at 1.5 GPa of standard peridotite residues and spinel lherzolites of 1,265 and 1,315°C, respectively. Depending on pressure and composition, similar temperatures in the range of approximately 1,200−1,300°C have been estimated for solidi of ultramafic rocks in the spinel stability field (e.g. Jaques and Green 1980; e.g. Baker and Stolper 1994; e.g. Katz et al. 2003; e.g. Wasylenki et al. 2003). Most peridotite samples associated with mid-ocean ridge systems are equilibrated to temperatures of $\sim 800 - 1,300°C$ (Hellebrand et al. 2005). Therefore, 800°C is used as lowest temperature when using the models, a rough approximation of a minimal closure temperature. However, it should be kept in mind that, depending primarily on initial temperatures and cooling rates, not all residues of mantle melting show the same equilibrium temperature. Furthermore, varying velocities of different diffusion processes could lead to individual deviations from equilibrium with decreasing temperature.

As already mentioned, the majority of expressions for K_D used in this study show insignificant pressure dependence and therefore do not account for pressure changes (Witt-Eickschen and Seck 1991; Witt-Eickschen and O'Neill 2005). Pressure is thus assumed to be a constant value of 1.5 GPa throughout the models. This choice has been made because (i) partial mantle melting beneath mid-ocean ridges is usually initiated at pressures between ~ 3.5 and ~ 1.5 GPa (Klein 2003), leading to a rough estimate for subsolidus reactions of 1.5 GPa and (ii) all distribution coefficients that are used in the final model are calibrated to temperatures calculated by the authors assuming 1.5 GPa.

Approach

In order to understand the effects of subsolidus reactions on the $Cr\#^{sp}$, the distribution of Al and Cr between all relevant mineral phases has to be modeled as a function of temperature. Since various reactions are proceeding at the same time, they have to be modeled simultaneously.

The most extensive and widely used internally consistent thermodynamic database is the one of Holland and Powell (Holland and Powell 1998). This database, however, does not contain chromium. The also widely used software package MELTS (Ghiorso and Sack 1995) for the thermodynamic modeling of phase equilibria assigns all chromium to spinel (Asimow and Ghiorso 1998). We therefore choose an approach that includes temperature-dependent Al-Cr distribution coefficients estimated from natural samples. The $Cr\#^{sp}$ in spinel-bearing mantle rocks is then modeled with an equation system composed of K_D expressions as function of temperature for each reaction. However, these equations contain a higher number of unknown variables than the number of equations. Hence, mass balance equations have to be included in addition ("Mass balance equations"). In this work, the creation of the final model was carried out as stepwise addition of reactions to the model, and this is described in "Ion-exchange reactions" and "Solubility of aluminum in orthopyroxene". At some points in this process, a preliminary model was applied to exemplary data in order to evaluate the importance of a reaction or the difference between different published distribution coefficients. The individual reactions require different mass balance restrictions, and these are described along with the corresponding model.

Implementation

From a mathematical viewpoint, all models described below essentially require the solution of a non-linear equation system with an equal number of equations and unknowns. Since, due to transcendental terms within the

equations, no solutions could be found analytically, numerical methods were used to solve the equation systems.

Solutions were computed in Mathematica (Wolfram Research, Inc. 2008) using the `FindRoot` function. This function essentially uses a modified Newton's Method with a backtracking strategy for the Newton step (Dennis Jr. and Schnabel 1996) as a globally convergent method. Using measured concentrations as starting parameters, convergent solutions have been obtained at all times. In some cases, the `DampingFactor` option had to be set to values <1 in order to produce robust results with the required precision.

Except for one equilibrium expression, only molar fractions are used in equations of the models. In order to minimize computational effort, all input data were converted to mole fractions values beforehand. Conversion was also done in Mathematica, using relations summarized in Deer et al. (1996). For some modal compositions, no indication whether the data are presented as wt% or vol% is given in the corresponding publication. Considering the small variations in mineral densities in ultramafic rocks, these modal compositions were taken directly as wt% because of the insignificant error due to the potentially omitted density conversion.

Mass balance equations

The assumption of a closed system yields mass balance equations for the components involved in reactions. For a component A,

$$\mathrm{A}^{\mathrm{opx}} \cdot X^{\mathrm{opx}} + \mathrm{A}^{\mathrm{cpx}} \cdot X^{\mathrm{cpx}} + \mathrm{A}^{\mathrm{sp}} \cdot X^{\mathrm{sp}} + \mathrm{A}^{\mathrm{ol}} \cdot X^{\mathrm{ol}} = const \tag{7}$$

where X^p is the mole fraction of mineral p, and A^p is the mole fraction of component A per formula unit of p. Thus, the sum in Eq. (7) is equal to the total number of moles of component A divided by the total number of moles of all components in the sample. For example, the mass balance equation for Al_2O_3 is

$$NB^{\mathrm{opx}}_{\mathrm{Al_2O_3}} + NB^{\mathrm{cpx}}_{\mathrm{Al_2O_3}} + NB^{\mathrm{sp}}_{\mathrm{Al_2O_3}} + NB^{\mathrm{ol}}_{\mathrm{Al_2O_3}} = const \tag{8}$$

where $NB^{\mathrm{p}}_{\mathrm{A}} \equiv \mathrm{A}^{\mathrm{p}} \cdot X^p$, and a similar equation can be formulated for Cr_2O_3. In other words, $N\,B^{\mathrm{p}}_{\mathrm{A}}$ is the number of moles of component A in phase p divided by the total number of moles of all components in the sample. When modeling the reaction changing the solubility of Al in opx, mass balance equations for MgO and SiO_2 have to be considered additionally.

Depending on the reactions, additional mass balance equations have to be considered. These are listed later in the corresponding sections.

Ion-exchange reactions

Orthopyroxene–spinel

The equilibrium distribution of Al and Cr between opx and sp (reaction (2)) can be described by the distribution coefficient

$$K_D^{\mathrm{opx/sp}} = \frac{x^{\mathrm{opx}}_{\mathrm{Al_2O_3}} \Big/ x^{\mathrm{opx}}_{\mathrm{Cr_2O_3}}}{x^{\mathrm{sp}}_{\mathrm{Al_2O_3}} \Big/ x^{\mathrm{sp}}_{\mathrm{Cr_2O_3}}}. \tag{9}$$

Witt-Eickschen and O'Neill (2005) analyzed the composition of 16 natural spinel lherzolite samples in order to determine K_D as a function of temperature. These well equilibrated samples show equilibrium temperatures (Ca-in-opx geothermometer of Brey and Köhler (1990) at 1.5 GPa) from 1150 to 1500 K and therefore, span a useful range of temperatures. The authors determined

$$\ln K_D^{\mathrm{opx/sp}} = \frac{1215 + 3137 Cr\#^{\mathrm{sp}}}{T} - 0.391 \tag{10}$$

with $\chi^2_v = 0.74$. The term with the $Cr\#^{\mathrm{sp}}$ accounts for the non-ideal miscibility of Al and Cr in spinel and is in good agreement with estimations of Klemme and O'Neill (2000).

No parameter errors are published for the fitting procedure, and uncertainties for the analysis of main element concentrations are not available. Thus, the fitting could not be reproduced exactly. However, when using a relative uncertainty of 5% for K_D (which is the value Witt-Eickschen and O'Neill (2005) used when uncertainties where not available) and otherwise unchanged details of the fitting procedure, a similar result is obtained. Absolute parameter errors for the published fit can then be estimated using the same relative parameter errors, yielding

$$\ln K_D^{\mathrm{opx/sp}} = \frac{1215(\pm 158) + 3137(\pm 150) Cr\#^{\mathrm{sp}}}{T} - 0.391(\pm 0.120). \tag{11}$$

Clinopyroxene–orthopyroxene

Using additional experimental data, Witt-Eickschen and O'Neill (2005) also determined

$$\ln K_D^{\mathrm{cpx/opx}} = \ln \left(\frac{x^{\mathrm{cpx}}_{\mathrm{Al_2O_3}} \Big/ x^{\mathrm{cpx}}_{\mathrm{Cr_2O_3}}}{x^{\mathrm{opx}}_{\mathrm{Al_2O_3}} \Big/ x^{\mathrm{opx}}_{\mathrm{Cr_2O_3}}} \right) = \frac{-1141 - 2302 \mathrm{Na}^{\mathrm{cpx}}}{T} + 0.905 \tag{12}$$

for the distribution between cpx and opx. Formulated with the enstatite and diopside endmembers, the corresponding reaction is

$$\underset{\text{opx}}{MgAl_2SiO_6} + \underset{\text{cpx}}{CaCr_2SiO_6} \rightleftharpoons \underset{\text{opx}}{MgCr_2SiO_6} + \underset{\text{cpx}}{CaAl_2SiO_6}. \quad (13)$$

Calculated temperatures predicted by equation (12) for the dataset of the authors result in values quite different from the temperatures used for the fitting procedure of the authors (differences of up to 670 K). Therefore, an attempt was made to find a new fit for equation (12).

Due to the lack of other data for Al/Cr partitioning between cpx and opx in the literature, a new fit was calculated for similar conditions. The data comprise of the 16 natural samples presented by Witt-Eickschen and O'Neill (2005) and 54 compositions from experimental studies cited therein (Falloon et al. 1999; Pickering-Witter and Johnston 2000; Schwab and Johnston 2001; Liu and O'Neill, 2004). Only plagioclase-free samples containing opx, cpx, ol, and sp were selected. Both xenolith and experimental samples display large variations in errors originating from analytic uncertainties (Fig. 1). All data are then fitted to

$$\ln K_D^{\text{cpx/opx}} = a + \frac{b + c \cdot \text{Na}^{\text{cpx}}}{T_{(\text{opx},1.5\,\text{GPa})}} \quad (14)$$

with parameters a, b and c. All temperatures are calculated using the Ca-in-opx geothermometer

$$T_{(\text{opx},P)} = \frac{6425 + 26.4P(\text{kbar})}{-\ln \text{Ca}^{\text{opx}} + 1.843} \quad (15)$$

of Brey and Köhler (1990) at 1.5 GPa. Using calculated $T_{(\text{opx}}$, 1.5 GPa) values rather than given experimental temperatures improved the fit significantly, suggesting incomplete equilibrium for pyroxenes in some experimental charges. The weighted non-linear least squares fit is calculated accounting for uncertainties in $\ln K_D$ and $\pm$ 10 K in T. Errors for $\ln K_D$ are calculated using given analytic errors. For the 16 natural samples, these values can be estimated from Fig. 16 in the corresponding publication. Fitting of the 70 data points then gives

$$\ln K_D^{\text{cpx/opx}} = \frac{-1395(\pm 121) - 1036(\pm 330)\text{Na}^{\text{cpx}}}{T} + 0.7933(\pm 0.0723) \quad (16)$$

($\chi_v^2 = 1.48$, T in Kelvin) as new distribution coefficient, which is used for further modeling. The improvement of this expression compared to Eq. (12) is displayed in Fig. 2.

In order to estimate the difference between $K_D^{cpx/opx}$ and partition coefficients available in literature, geothermometers developed by Hervig and Smith (1982) and Seitz et al. (1999) have been considered additionally. Seitz et al. (1999) obtained

$$T(K) = \frac{11.00 \cdot P + 2829}{1.56 - \ln D_{\text{Cr}}^{\text{opx/cpx}}} \quad (17)$$

where P is the pressure in kbar and $D_{\text{Cr}}^{\text{opx/cpx}} = [\text{Cr}]_{wt}^{\text{opx}}/[\text{Cr}]_{wt}^{\text{cpx}}$. Hervig and Smith (1982) determined partition coefficients for Cr between ol/cpx and opx/ol. The combination of these two partition coefficients gives

$$D_{\text{Cr}}^{\text{cpx/opx}} = \frac{[\text{Cr}]_{wt}^{\text{cpx}}}{[\text{Cr}]_{wt}^{\text{opx}}} = 0.36422 \cdot \exp\frac{3247}{T} \quad (18)$$

with T in K.

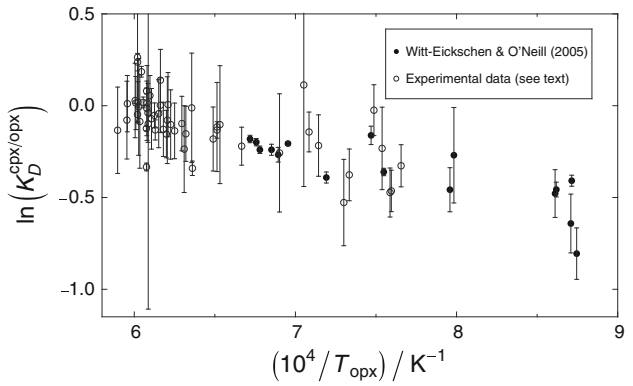

Fig. 1 Plot of $10^4/T_{\text{opx}}$ (Ca-in-opx geothermometer of Brey and Köhler 1990) versus $\ln K_D^{\text{cpx/opx}}$ of the xenolith samples of Witt-Eickschen and O'Neill (2005) (*closed circles*) and various experimental data (*open circles*, see text). *Error bars* display errors resulting from analytic uncertainties

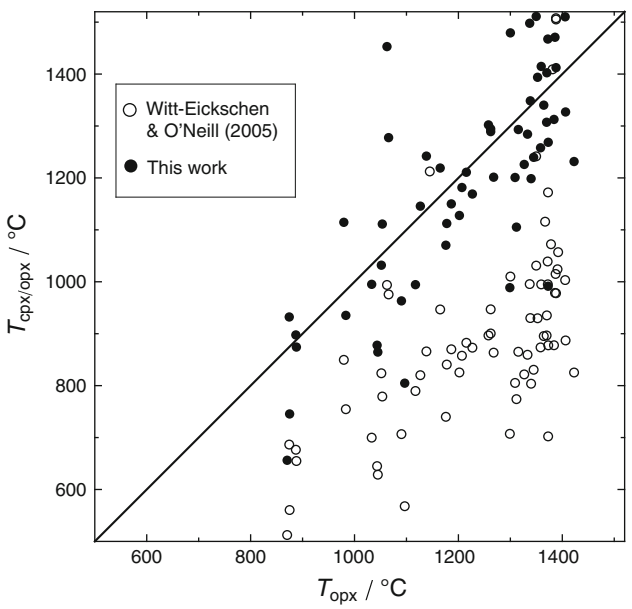

Fig. 2 Plot of T_{opx} (Ca-in-opx geothermometer of Brey and Köhler 1990) versus $T_{\text{cpx/opx}}$. *Open circles* represent temperatures calculated according to $K_D^{\text{cpx/opx}}$ of Witt-Eickschen and O'Neill (2005), whereas the *closed circles* represent Eq. (16) in this work. Temperatures are expected to fall on a 1:1 line because T_{opx} was used to calibrate $K_D^{\text{cpx/opx}}$

In order to demonstrate differences between geothermometers described in Eqs. (16, 17, 18), they have been included into a preliminary model along with $K_D^{opx/sp}$ (Eq. 11). Additionally to the general mass balance equations, the sums $\left(NB^{p}_{Al_2O_3} + NB^{p}_{Cr_2O_3}\right)$ with p = opx,cpx,sp are assumed to be constant at this point. The application of this preliminary model to a spinel peridotite composition (Fig. 3) reveals differences between these geothermometers. Since $K_D^{cpx/opx}$ should be valid in a more general scenario than the partition coefficients, only the recalculated cpx/opx distribution coefficient (Eq. 16) is used in further models.

Olivine–spinel

Olivine only shows a very limited ability to include Al and Cr in its crystal lattice, demonstrated by Cr contents below 1,000 ppm (Witt-Eickschen and O'Neill, 2005) and Al contents below 200 ppm (Wan et al. 2008) in spinel peridotites. Nevertheless, the high olivine content of peridotites requires the examination of Al/Cr partitioning between olivine and other minerals.

Due to the poor correlation between Cr^{ol} and the $Cr\#^{sp}$, Witt-Eickschen and O'Neill (2005) propose the reaction

$$\underset{sp}{\frac{1}{2}MgCr_2O_4} + \underset{sp}{\frac{1}{2}MgAl_2O_4} \rightleftharpoons \underset{ol}{MgCrAlO_4} \quad (19)$$

instead of an exchange similar to those described above for opx, sp, and cpx. The poor correlation may also be due to analytical problems at low Cr contents in their samples or prevailing temperature effects because of a narrow compositional range as discussed by Ionov (2007).

Reaction (19) induces a proportionality $Cr^{ol} \propto Cr\#^{sp}(1 - Cr\#^{sp})$, apparently leading to a better fit

$$\ln Cr^{ol} = \ln(Cr\#^{sp}(1 - Cr\#^{sp})) - 10070/T + 14.47 \quad (20)$$

where Cr^{ol} is given in ppm. Still, χ^2_ν is 5.3, and the influence of Al in olivine was not determined, impeding further analysis.

In order to determine whether reaction (19) is important or not, it can be modeled simultaneously with the cpx–opx and opx–sp equilibria ("Clinopyroxene–orthopyroxene" and "Orthopyroxene–spinel", respectively). This requires the introduction of additional mass balance equations

$$NB^{p}_{Al_2O_3} + NB^{p}_{Cr_2O_3} = const\ (p = \text{opx}, \text{cpx}) \quad (21a)$$

$$X^{ol} + X^{sp} = const \quad (21b)$$

$$\Delta NB^{ol}_{Al_2O_3} = \Delta NB^{ol}_{Cr_2O_3} \quad (21c)$$

$$\Delta NB^{ol}_{MgO} = 0.5\Delta NB^{ol}_{Al_2O_3} \quad (21d)$$

$$\Delta X^{ol} = 0.5\Delta NB^{ol}_{Al_2O_3} \quad (21e)$$

where variables preceded by Δ are changes in these variables due to modeled reactions.

The resulting preliminary model is then applied to sample MM1213 of Witt-Eickschen and O'Neill (2005) which shows a high olivine content of 84 wt%. A comparison to the results obtained without ol/sp partitioning ("Clinopyroxene–orthopyroxene", solid and dashed lines in Fig. 4) shows that variations in the $Cr\#^{sp}$ caused by Al/Cr exchange in olivine can be neglected even for high olivine contents.

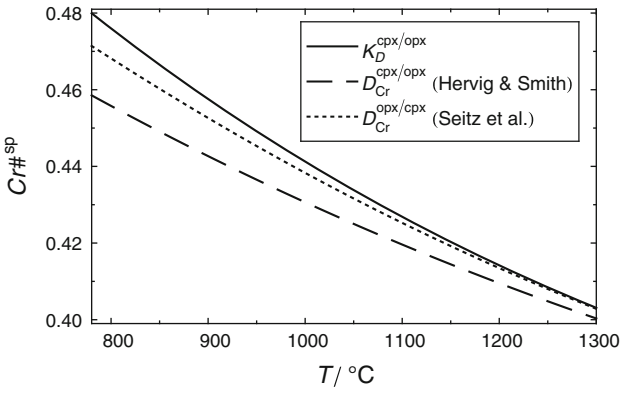

Fig. 3 The calculated $Cr\#^{sp}$ of lherzolite sample MM1260 of Witt-Eickschen and O'Neill (2005) as result of preliminary models with different $K_D^{cpx/opx}$ (see "Clinopyroxene–orthopyroxene"). The *solid line* results from a model incorporating distribution coefficients for opx/sp and cpx/opx (recalculated) equilibria by the same authors. Combining data for partitioning of Cr of Hervig and Smith (1982) with $K_D^{cpx/opx}$ gives the *dashed line*, whereas the combination with data of Seitz et al. (1999) gives the *dotted line*

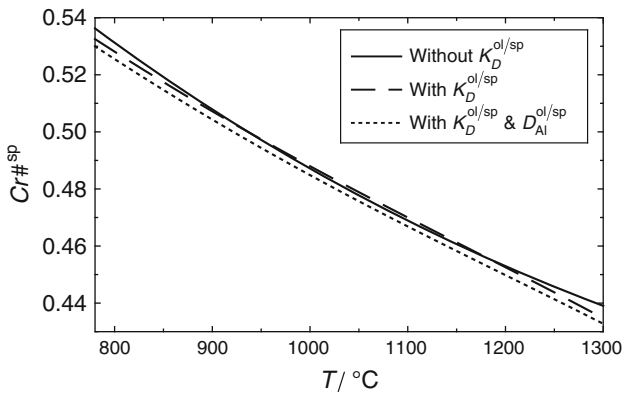

Fig. 4 The $Cr\#^{sp}$ of harzburgite sample MM1213 (84 wt% ol) of Witt-Eickschen and O'Neill (2005) as result of different preliminary models. Including Al/Cr partitioning between ol and sp (*dashed line*) into the model (*solid line*) only leads to negligible changes. The *dotted line* is obtained when the Al partitioning between ol and sp according to Wan et al. (2008) is combined with $K_D^{ol/sp}$

A similar result is obtained, when the ol/sp partitioning is described using the results of Wan et al. (2008)

$$T(^{\circ}\mathrm{C}) = \frac{10000}{0.512 + 0.873 \cdot Cr\#^{sp} - 0.91 \ln D_{Al}^{ol/sp}} - 273 \quad (22)$$

where $D_{Al}^{ol/sp} = [Al_2O_3]_{wt}^{ol}/[Al_2O_3]_{wt}^{sp}$ (dotted line in Fig. 4). Even though there are slightly larger differences, they are still not significant. The partitioning of Al and Cr between olivine and spinel is therefore not included in further modeling.

Solubility of aluminum in orthopyroxene

As it will be recognizable from the results, incorporating changes in the solubility of Al in opx is important for a realistic model. The net-transfer reaction describing this process (Tschermak exchange in opx)

$$\underset{sp}{MgAl_2O_4} + \underset{opx}{Mg_2Si_2O_6} \rightleftharpoons \underset{ol}{Mg_2SiO_4} + \underset{opx}{MgAl_2SiO_6} \quad (23)$$

leads to an equilibrium constant of a different form than for the simple ion-exchange reactions discussed above. According to Stroh (1976),

$$K^{Ts-Opx} = \frac{a_{Mg_2SiO_4}^{ol} \cdot a_{MgAl_2SiO_6}^{opx}}{a_{MgAl_2O_4}^{sp} \cdot a_{Mg_2Si_2O_6}^{opx}} = \underbrace{\frac{\left(x_{Mg}^{M}\right)_{ol}^{2} \cdot \left(x_{Al}^{M1}\right)_{opx}}{\left(x_{Mg}^{A}\right)_{sp} \cdot \left(x_{Al}^{B}\right)_{sp}^{2} \cdot \left(x_{Mg}^{M1}\right)_{opx}}}_{K_D^{Ts-Opx}} \cdot K_\gamma \quad (24)$$

where $(x_A^S)_p$ is the mole fraction of component A on the crystallographic site S in phase p. In practice, fractions of Mg and Al on the M1 site in opx are calculated using

$$\left(x_{Al}^{M1}\right)_{opx} = \frac{Al^{opx} + Na^{opx} - 2Ti^{opx} - Cr^{opx}}{2} \quad (25a)$$

$$\left(x_{Mg}^{M1}\right)_{opx} = \frac{1}{4}(2Mg^{opx} + 2Mn^{opx} + 2Ca^{opx} + 2Ti^{opx} + Na^{opx} - Al^{opx} - Cr^{opx}) \quad (25b)$$

according to Gasparik and Newton (1984). As no detailed specifications are given in publications of corresponding geothermometers,

$$\left(x_{Mg}^{M}\right)_{ol} = \frac{Mg^{ol}}{Mg^{ol} + Fe^{ol}} \quad (26a)$$

$$\left(x_{Mg}^{A}\right)_{sp} = \frac{Mg^{sp}}{Mg^{sp} + Fe^{sp}} \quad (26b)$$

$$\left(x_{Al}^{B}\right)_{sp} = \frac{Al^{sp}}{Al^{sp} + Cr^{sp}} \quad (26c)$$

is assumed here.

Several geothermometers based on this equilibrium exist today. While the equation of Gasparik and Newton (1984)

$$RT \ln K_D^{Ts-Opx} + 29190 - 13.42T + 0.18T^{1.5} + (0.013 + 3.34 \cdot 10^{-5}(T - 298) - 6.6 \cdot 10^{-7}P)P = 0 \quad (27)$$

with P in bar, R in $J\,K^{-1}mol^{-1}$, and T in K is not accounting for deviations from ideality in the spinel solid solution, the expression of Witt-Eickschen and Seck (1991)

$$T = 2248.25 + 991.58 \ln K_D^{Ts-Opx} + 153.32\left(\ln K_D^{Ts-Opx}\right)^2 + 539.05 Cr\#^{sp} - 2005.74(Cr\#^{sp})^2 \quad (28)$$

with T in °C incorporates $Cr\#^{sp}$ terms accounting for this non-ideality. Hence, the second equation should give a more accurate result. Moreover, this equation is calibrated to the same geothermometer (Ca-in-opx of Brey and Köhler (1990)) as the K_D expressions described above, promoting a more consistent model. According to the authors, (28) reproduced temperatures within ±20°C, which is used as uncertainty here.

The addition of this reaction to those described earlier again requires specific mass balance equations:[1]

$$NB_{Al_2O_3}^{cpx} + NB_{Cr_2O_3}^{cpx} = const \quad (29a)$$

$$X^{ol} + X^{sp} = const \quad (29b)$$

$$\Delta NB_{SiO_2}^{opx} = -\Delta X^{ol} \quad (29c)$$

$$\Delta N_{SiO_2}^{opx} = \Delta NB_{MgO}^{opx} \quad (29d)$$

$$\Delta X^{sp} = \Delta NB_{MgO}^{sp} \quad (29e)$$

$$\Delta X^{sp} = \Delta NB_{Al_2O_3}^{sp} + \Delta NB_{Cr_2O_3}^{sp} \quad (29f)$$

Together with $K_D^{opx/sp}, K_D^{cpx/opx}, K_D^{Ts-Opx}$ and mass balance equations according to "Mass balance equations", there is now a total of 13 equations in this final model. The difference between Eqs. (27) and (28) is shown in Fig. 5.

Estimation of uncertainties

Since equilibrium concentrations are obtained by a numerical solution, the propagation of errors in input parameters cannot be calculated deterministically. Thus, the Monte Carlo Simulation is an adequate tool to estimate uncertainties in modeled values. As uncertainties in the starting composition for the model would simply cause a systematic shift of the modeled $Cr\#^{sp}$, these errors are not

[1] The term $-\Delta NB_{Cr_2O_3}^{sp}$ is the amount of $\Delta NB_{Al_2O_3}^{sp}$ due to the $K_D^{opx/sp}$ equilibrium reaction (2), and therefore this term has to be subtracted in the last equation.

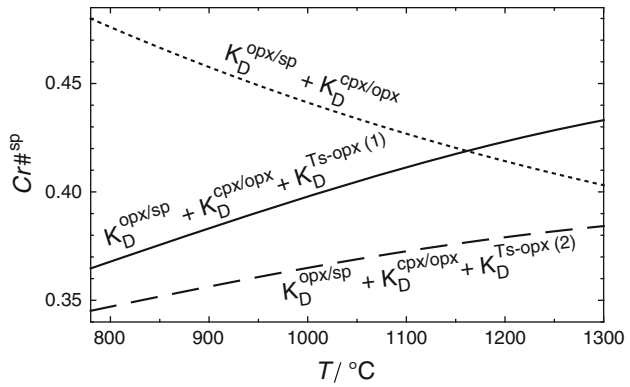

Fig. 5 The $Cr\#^{sp}$, resulting from the application of the final model (*solid line*) using $K_D^{\text{Ts-opx (1)}}$ of Witt-Eickschen and Seck (1991) and the model using the less accurate $K_D^{\text{Ts-opx (2)}}$ of Gasparik and Newton (1984) (*dashed line*) to lherzolite sample MM1260 of Witt-Eickschen and O'Neill (2005). The final model incorporates the effects of opx-sp exchange (see "Orthopyroxene–spinel"), minor effects of opx-cpx exchange (see "Clinopyroxene–orthopyroxene") and dominant control of the Tschermak exchange in opx (see "Solubility of aluminum in orthopyroxene"). For comparison, the results of the application of the same data without reaction (23) (*dotted line*, *solid line* in Fig. 3) is included

included in error estimations—only uncertainties in the geothermometers described above have been included.

Monte Carlo Simulations were evaluated assuming normal distributions for all uncertainties and 10000 runs in order to produce robust results.

Resulting errors are displayed as error bars. It should be kept in mind, that when comparing the $Cr\#^{sp}$ at two different temperatures, possible variations due to uncertainties occur in the same way at both temperatures. For example, a shift to higher chromium numbers at a low temperature would occur likewise at higher temperatures. In other words, the absolute shift of the curves to higher or lower chromium numbers due to uncertainties affects its change between two temperatures only in a minor way.

Inevitably, error bars suggest that there is no significant difference of the $Cr\#^{sp}$ between two temperatures in some cases. Thus, the variation in the $Cr\#^{sp}$ between 800 and 1,300°C and the corresponding uncertainty is presented in addition to the diagrams.

Results

In order to evaluate possible effects of the modeled processes, it is crucial to apply the final model to different initial compositions. Therefore, the $Cr\#^{sp}$ is calculated for several natural xenolith samples presented in Witt-Eickschen and O'Neill (2005). All of them are well equilibrated, and therefore application of the model produces reasonable results. In addition, a natural websterite sample from the Southwest Indian Ridge (D47-12), previously described by Dantas et al. (2007), is used.

Important compositional parameters and temperatures calculated with various geothermometers which were used in the modeling process are listed in Table 1. Differences in calculated temperatures with a maximum of ±74°C are observable. The discrepancies between the Ca-in-opx geothermometer of Brey and Köhler (1990) and temperatures according to $K_D^{\text{opx/sp}}$ and $K_D^{\text{cpx/opx}}$ are in the range of one standard deviation (1σ) of these geothermometers. Besides, there is no apparent correlation of temperatures with $Cr\#^{sp}$ when a larger set of samples is considered, and as a consequence these errors should largely be of a random nature.

In contrast, temperatures calculated with $K_D^{\text{Ts-Opx}}$ (Eq. (28)) exhibit systematically lower values. This phenomenon has been noticed in other natural samples (e.g. Franz et al, 1997). Klemme and O'Neill (2000) noticed that this phenomenon also exists with experimental data. Hence, the parameters calculated here may exhibit a systematic shift. Nevertheless, the trend and magnitude of changes in the $Cr\#^{sp}$ should be independent of this deficiency.

Lherzolites

The sample Mo22 is used as an example for a relatively fertile spinel lherzolite. The low olivine content, a

Table 1 Petrographic properties and calculated equilibrium temperatures of selected ultramafic samples

Sample	Mode/wt%				$Cr\#^{sp}$	X_{Mg}^{ol} [a]	T/°C			
	ol	opx	cpx	sp			Ca-in-opx[b]	$K_D^{\text{opx/sp}}$[c]	$K_D^{\text{cpx/opx}}$[d]	$K_D^{\text{Ts-Opx}}$[e]
MM1260[f]	73	20	5	2	0.418	0.917	1207 ± 19	1173 ± 139	1182 ± 162	1158 ± 20
MM1213[f]	84	13	2	1	0.451	0.921	1202 ± 19	1205 ± 139	1128 ± 154	1140 ± 20
DW1342[f]	86	8	3	2	0.411	0.916	1165 ± 19	1185 ± 142	1219 ± 164	1124 ± 20
Mo22[f]	63	21	14	3	0.108	0.896	1052 ± 19	1052 ± 205	1110 ± 136	1007 ± 20
D47-12[g]	–	50	45	5	0.156	–	991 ± 19	1085 ± 182	962 ± 131	–

[a] Molar Mg/(Mg+Fe) in olivine; [b] Eq. (15) in text at 1.5 GPa; [c] Eq. (11) in text; [d] Eq. (16) in text; [e] Eq. (28) in text; [f] Analytical data is given in Witt-Eickschen and O'Neill (2005); [g] Analytical data is given in Dantas et al. (2007)

relatively small X_{Mg}^{ol} and a low Cr content indicate that only small amounts of basaltic melt have been extracted from this xenolith (Preß et al. 1986). These petrographic and geochemical properties are characteristic features of the DMM, similar to those presented by Workman and Hart (2005).

The change of the $Cr\#^{sp}$ indicated by application of the model (Fig. 6) between 1,300 and 800°C is only -0.0096 ± 0.0043. Nevertheless, this is a significant decrease (greater than 1σ) in the $Cr\#^{sp}$. The original $Cr\#^{sp}$ of 0.108 at 1,052°C lies in the range of 1σ of the calculated $Cr\#^{sp}$ at the same temperature, which is 0.112 ± 0.008.

A plot of the spinel mode (inset in Fig. 6) suggests that spinel is constantly growing during cooling. Inevitably, the amount of olivine in the rock would decrease by the same magnitude during cooling according to the model (see reaction (23)). This is in agreement with thermodynamic modeling of Coogan et al. (2007) using MELTS (Ghiorso and Sack, 1995), predicting the growth of spinel along with a decreasing $Cr\#^{sp}$ during cooling.

Harzburgites

Abyssal harzburgites are representative of mantle rocks which were subjected to melt extraction. Sample MM1213, a spinel harzburgite, shows typical properties of such a rock. In comparison with Mo22, this xenolith contains a larger amount of olivine along with a higher X_{Mg}^{ol} and a much greater chromium content.

Figure 7 illustrates the calculated $Cr\#^{sp}$ and spinel mode for this sample, indicating a much greater decrease in the chromium number with this configuration. Between 1,300 and 800 °C, a decrease of -0.0823 ± 0.0126 in the $Cr\#^{sp}$ is predicted. At 1202°C, which is the temperature according to the Ca-in-opx geothermometer of Brey and Köhler (1990), the calculated chromium number is 0.465 ± 0.013. Since the original $Cr\#^{sp}$ is 0.451, the calculated value is systematically higher. The reason for this effect is most likely the underestimation of temperatures by the $K_D^{Ts\text{-}Opx}$-geothermometer as described above.

Similar to the trend in the lherzolite, spinel is predicted to grow during cooling in this harzburgite (inset in Fig. 7). However, the absolute change is smaller, owing to the smaller absolute spinel fraction in the rock.

Clinopyroxene-bearing dunites

Clinopyroxene-bearing dunites are typical for crust-mantle transition zone dunites in the Oman ophiolite (Boudier and Nicolas 1995). These dunites are usually interpreted as conduits for melt flow (Kelemen et al. 1995). Although sample DW1342 is not a dunite sensu stricto, it is suitable as a representation of this rock type.

Using the model created in this work, the curves in Fig. 8 are obtained. The calculated $Cr\#^{sp}$ at 1,165°C of 0.416 ± 0.007 is in agreement with the measured value of 0.411. As illustrated in Fig. 8, the $Cr\#^{sp}$ is predicted to decrease only by -0.0364 ± 0.0046 between 1,300 and 800°C. This is less than half of the corresponding value of the harzburgite sample, which shows approximately the same absolute chromium content. The main reason for this is the lower opx content of this rock, which influences the $K_D^{Ts\text{-}Opx}$ equilibrium.

Websterites

In contrast to the previous rock types, websterites contain large amounts of pyroxene and only a small fraction of olivine. Sample D47-12 of Dantas et al. (2007), containing no olivine at all, was chosen as representation of this

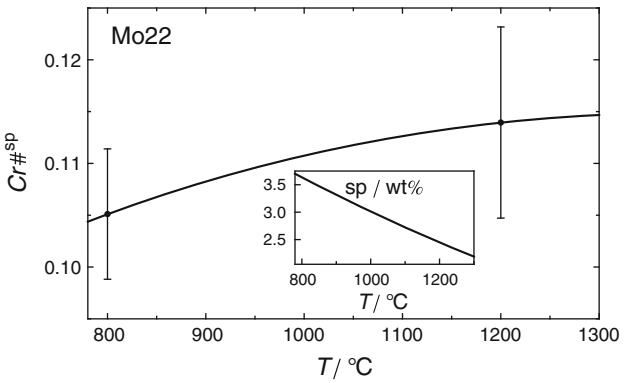

Fig. 6 Plot of calculated $Cr\#^{sp}$ and wt% spinel (*inset*) of fertile lherzolite sample Mo22, indicating a decrease in the $Cr\#^{sp}$ of only -0.0096 from 1,300 to 800°C. Errors are calculated from uncertainties (1σ) in K_D expressions

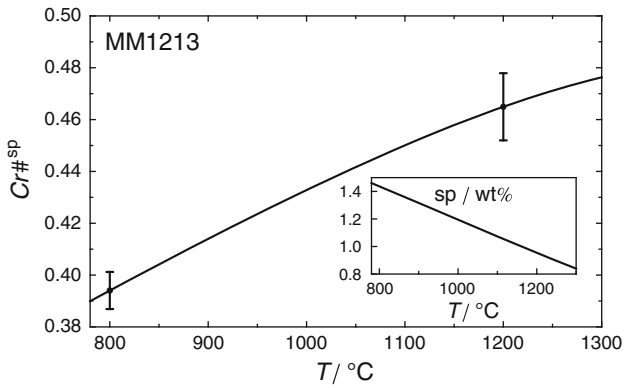

Fig. 7 Plot of calculated $Cr\#^{sp}$ and wt% spinel (*inset*) of harzburgite sample MM1213, indicating a decrease in the $Cr\#^{sp}$ of -0.0823 from 1,300 to 800°C. Errors are calculated from uncertainties (1σ) in K_D expressions

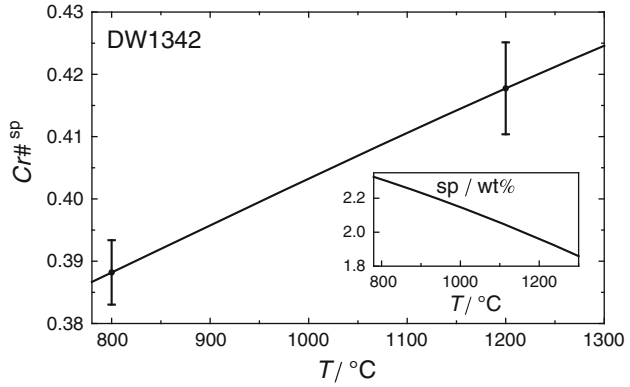

Fig. 8 Plot of calculated $Cr\#^{sp}$ and wt% spinel (*inset*) of clinopyroxene-bearing dunite sample DW1342, indicating a decrease in the $Cr\#^{sp}$ of −0.0364 from 1,300 to 800°C. Errors are calculated from uncertainties (1σ) in K_D expressions

ultramafic rock type. This sample is equilibrated to 991°C and shows a low $Cr\#^{sp}$ of 0.156. Application of the model gives a $Cr\#^{sp}$ of 0.166 ± 0.014 at the same temperature, which lies in the range of 1σ of the original value. Due to the low olivine content, this sample is predicted to show a different behavior during cooling than the previous samples (Fig. 9).

According to $K_D^{\text{Ts-Opx}}$, olivine would be present above 984°C (inset in Fig. 6). At lower temperatures, no olivine is predicted to be present and the $Cr\#^{sp}$ would therefore increase during further cooling. Hence, $\Delta Cr\#^{sp}$ from 1300 to 800°C is predicted to increase slightly by 0.0034 ± 0.0033.

However, we cannot be certain that olivine-out did not occur at a higher temperature, which would shift the position of the kink in the model (Fig. 9) to higher

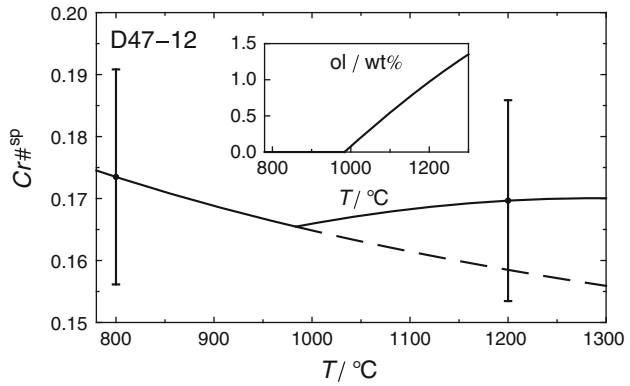

Fig. 9 Plot of calculated $Cr\#^{sp}$ and wt% olivine (*inset*) of websterite sample D47-12 (*solid line*). At temperatures above 984°C, $K_D^{\text{Ts-Opx}}$ predicts that olivine is present in the rock. The projected $Cr\#^{sp}$ evolution trend if no olivine is present is shown as *dashed line*. The respective error bar at 1,200°C would be of similar size. During cooling from 1,300 to 800°C, the $Cr\#^{sp}$ is predicted to increase slightly by 0.0034 for the first case. If olivine was never present, $\Delta Cr\#^{sp}$ is 0.0176. Errors are calculated from uncertainties (1σ) in K_D expressions

temperatures. If olivine was never present in the websterite, this would result in a maximum $\Delta Cr\#^{sp}$ of 0.0176 ± 0.0050.

Discussion

The goal of this study was to investigate possible effects of subsolidus processes on the $Cr\#^{sp}$ occurring during cooling of ultramafic rocks. In particular, compositional zoning patterns observed in spinels and pyroxenes in abyssal peridotites give reason to evaluate the causative reactions in detail (Seyler et al. 2007; Coogan et al. 2007). The possibility of a significant influence of such processes has been described in the literature (e.g. Coogan et al. 2007), but has never been quantified. In this work, a model of important subsolidus reactions has been created and applied to a representative range of modal and chemical compositions of ultramafic rocks.

The results summarized in Table 2 suggest that there is indeed a significant change in the $Cr\#^{sp}$ to be expected due to the modeled reactions. Unfortunately, there is no reliable equilibrium expression for the solubility of Al in cpx, leading to potential uncertainties. Additionally, the geothermometer using the corresponding equilibrium in opx (Eq. 28) apparently gives systematically lower temperatures than other independent geothermometers.

Another potential source of uncertainty, the influence of Na concentration in cpx which is incorporated in the equation for cpx/opx (Eq. 16), has been evaluated by us. Sodium in cpx has been shown to be mobile in the mantle after melting and therefore may be distorted (e.g. Hellebrand and Snow 2003). We tested the effect of a secondary increase by 1 wt%, a typical value (Hellebrand and Snow 2003), on our results and found it insignificant.

Despite of these drawbacks, the trend and the change of the $Cr\#^{sp}$ over the temperature interval of 800−1,300°C still is a valuable approximation of the influence of subsolidus processes: In spinel peridotites, the $Cr\#^{sp}$ is predicted to decrease during cooling along with the growth of spinel. A MELTS model of Coogan et al. (2007) predicted qualitatively a similar trend for upper mantle rocks.

Table 2 Chromium numbers at different temperatures as predicted by application of the final model

Sample	$Cr\#^{sp}_{800°C}$	$Cr\#^{sp}_{1300°C}$	$Cr\#^{sp}_{800°C} - Cr\#^{sp}_{1300°C}$
MM1260	0.368 ± 0.007	0.433 ± 0.016	−0.0652 ± 0.0108
MM1213	0.394 ± 0.007	0.476 ± 0.017	−0.0823 ± 0.0126
DW1342	0.388 ± 0.005	0.425 ± 0.008	−0.0364 ± 0.0046
Mo22	0.105 ± 0.006	0.115 ± 0.010	−0.0096 ± 0.0043
D47-12	0.173 ± 0.017	0.170 ± 0.017	0.0034 ± 0.0033

Our model predicts an increase in spinel mass of up to 1.4 wt% for the pyroxene-rich lithologies (Mo22, D47-12) and around 0.5 wt% for the pyroxene-poor lithologies (MM1213, DW1342) during cooling. Harzburgite MM1260 falls in between with 1 wt%. A correlation exists between the initial spinel mode in Table 1 and $\Delta Cr\#^{sp}$ in Table 2: the negative change of the $Cr\#^{sp}$ is less pronounced at higher spinel modes (Fig. 10). This correlation results from partitioning of the cooling released chromium into a higher spinel volume. Clearly, there are other factors influencing this correlation, the opx/sp modal ratio probably being the most important factor.

The comparison of calculated chromium numbers in different rock types shows large differences in the magnitude of $\Delta Cr\#^{sp}$ between 1,300 and 800°C (Fig. 11). Apparently, there is a correlation between absolute values of chromium numbers and the predicted decrease in the $Cr\#^{sp}$ when considering lherzolites and harzburgites only. Namely, the decrease in the $Cr\#^{sp}$ is greater at higher absolute values of the chromium number. This is a very rough first approximation, which is not valid in a general scenario. For example, the low olivine content of websterites and pyroxenites has a large influence on the reactions, and a different behavior of the system is predicted by the model.

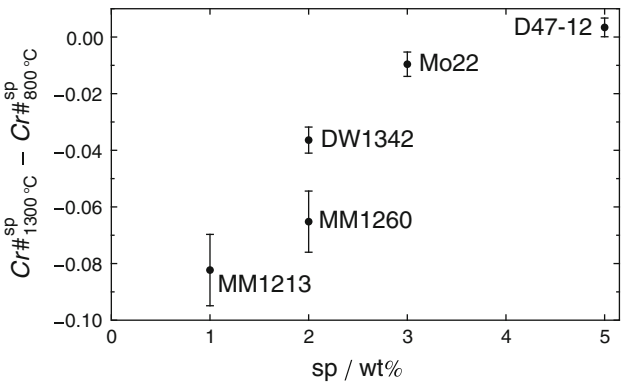

Fig. 10 Plot of $\Delta Cr\#^{sp}$ between 1,300 and 800°C resulting from the model created in this work versus wt% spinel. The different spinel peridotite samples of Witt-Eickschen and O'Neill (2005) presented in Table 1 show a correlation between these two values: the change of the $Cr\#^{sp}$ is less pronounced at higher spinel modes. Other factors, for example opx/sp ratios, may also show an effect. DW1342 with an opx/sp ratio of 13 shows a smaller change in $Cr\#^{sp}$ than MM1260 with opx/sp = 10 at a given spinel mode

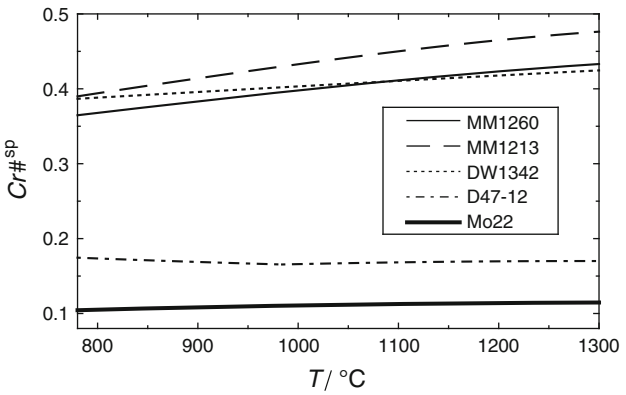

Fig. 11 Plot of T versus the calculated $Cr\#^{sp}$ of the selected samples. Apparently, $\Delta Cr\#^{sp}$ is greater at higher absolute chromium numbers in spinel peridotites (MM1260, MM1213, Mo22). Different behaviors are predicted for cpx-dunites (DW1342) and websterites (D47-12)

In order to parameterize the change in $Cr\#^{sp}$ at a given $Cr\#^{sp}$, a mathematical description of the correlation described above was developed. The Ca-in-opx temperatures of the samples used for the original fit of Hellebrand et al. (2001) are relatively high with a mean of $\sim$ 1270°C. Therefore, the possible effects when applying this equation to samples equilibrated to lower temperatures are evaluated here.

Fourteen spinel peridotite xenoliths of (Witt-Eickschen and O'Neill 2005) were used to obtain stable results. Two data points, DW1342 and DW211, have been excluded from this fitting procedure because of their special petrography. In addition, modeled DMM and harzburgite compositions developed by Workman and Hart (2005) have been included.

The presumably correlated parameters are displayed in Fig. 12. A linear regression with weights according to the errors gives

$$(Cr\#^{sp}_{1270°C} - Cr\#^{sp}_{800°C}) = -0.011(\pm 0.005) + 0.179(\pm 0.019) \cdot Cr\#^{sp}_{1270°C} \quad (30)$$

with $R^2 = 0.97$.

The change in $Cr\#^{sp}$ may have a potential effect on temperature estimates. Geothermometers utilizing the temperature-dependent Mg-Fe exchange between spinel and silicates assume a constant $Cr\#^{sp}$. If conversely a change in $Cr\#^{sp}$ through cooling would occur at a constant $K_D^{Mg/Fe}$ between silicates and spinel, this would translate into a downshift in calculated temperatures between about 10 and 65°C for the ol-sp geothermometer of Fabriès (Fabriès 1979) and 10 and 135°C for the opx-sp geothermometer of Liermann and Ganguly (2003, 2007) (at an initial $Cr\#^{sp}$ of 0.1 and 0.6, respectively). Obviously, the $K_D^{Mg/Fe}$ between silicates and spinel is not constant during cooling, and in fully equilibrated rocks, both coefficients would record the same equilibration temperature, hence no effect on temperature estimates would occur. However, due to the different diffusivities of Cr-Al (Suzuki et al. 2008) and Mg-Fe (Liermann and Ganguly 2002) in spinel, distortions may develop between the two values depending on the cooling

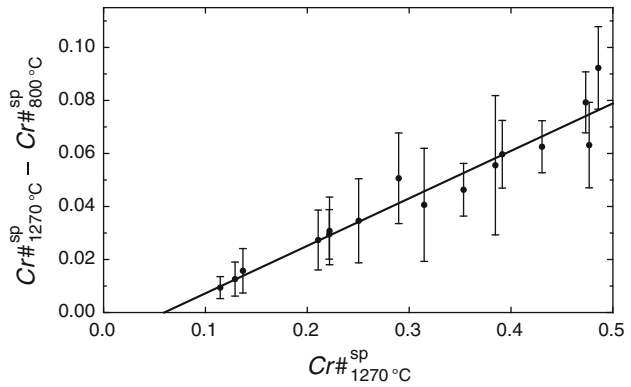

Fig. 12 Plot of $Cr\#^{sp}_{1270°C}$ vs. $\Delta Cr\#^{sp}$ between 800 and 1,270°C, both values predicted by the model created in this work. Since the equation of Hellebrand et al. (2001) which estimates the degree of partial melting (Eq. 31) is calibrated to rocks with a mean equilibration temperature of ~1,270°C, this temperature was chosen as upper temperature limit. Fourteen natural spinel peridotite samples of Witt-Eickschen and O'Neill (2005) are displayed along with modeled DMM and harzburgite compositions developed by Workman and Hart (2005). The line displays Eq. (30)

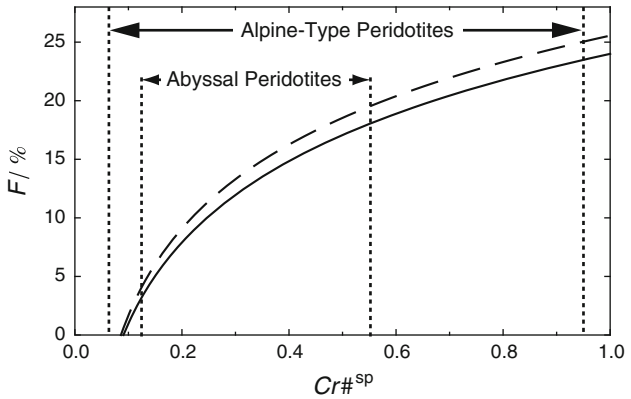

Fig. 13 Plot of the $Cr\#^{sp}$ versus the degree of partial melting F. The *solid line* represents the empirical equation of Hellebrand et al. (2001), which is calibrated to samples which show a high mean equilibration temperature of ~1,270°C. The dashed line illustrates the corrected value of F, if samples calibrated to 800°C would be applied to this equation. Compositional ranges of alpine-type and abyssal spinel peridotites of Dick and Bullen (1984) are marked for reference

rate and grain size as each equilibrium pair may record different closure temperatures.

Our regression can be also used to evaluate possible effects of cooling on the equation, which gives the degree of partial melting

$$F = 10\ln(Cr\#^{sp}) + 24 \quad (31)$$

of Hellebrand et al. (2001). If Eq. (31) would be applied to peridotites with equilibrium temperatures of 800°C, F would be underestimated by 1.50 ± 0.28% at $Cr\#^{sp}_{1270°C} = 0.6$, as illustrated in Fig. 13. Considering that this is an estimation of the maximum effects of the subsolidus processes, this a relatively small value. Therefore, the $Cr\#^{sp}$ is a robust parameter for the estimation of the degree of partial melting.

Conclusions

The chromium number in spinel is an important factor for the estimation of the degree of partial melting, temperatures, and provenance in ultramafic rocks but can potentially be affected by subsolidus processes. We developed a model to investigate the significance of ion-exchange and net-transfer reactions during cooling on this parameter and applied it to a relevant set of natural samples.

During cooling in the temperature range from 1,300 to 800°C, the application of the model created in this work predicts significant changes in the $Cr\#^{sp}$ in all investigated lithologies. When considering spinel lherzolites and harzburgites, the model predicts a decreasing $Cr\#^{sp}$ and growing spinel mass. The calculated decrease in $Cr\#^{sp}$ in cpx-dunites is smaller than in peridotites. In contrast, cooling of websterites is predicted to cause a slight increase in the $Cr\#^{sp}$ because of their lack of olivine. Apparently, the magnitude of the decrease in peridotites is greater at higher absolute values of the $Cr\#^{sp}$. This cooling effect only leads to minor potential changes when calculating the degree of partial melting as function of the $Cr\#^{sp}$ after Hellebrand et al. (2001) (up to ~1.5% in the chosen temperature range). Hence, using the $Cr\#^{sp}$ in mantle rocks for the evaluation of the degree of partial melting is a robust method.

Acknowledgments We would like to thank Zoran Jovanovic for discussion. Helpful comments from Dmitri Ionov and an anonymous reviewer are greatfully acknowledged.

References

Allan JF, Sack RO, Batiza R (1988) Cr-rich spinels as petrogenetic indicators; MORB-type lavas from the Lamont seamount chain, eastern Pacific. Am Mineral 73(7-8):741–753

Asimow PD, Ghiorso MS (1998) Algorithmic modifications extending MELTS to calculate subsolidus phase relations. Am Mineral 83:1127–1132

Baker MB, Stolper EM (1994) Determining the composition of high-pressure mantle melts using diamond aggregates. Geochim Cosmochim Acta 58(13):2811–2827

Barnes SJ, Roeder PL (2001) The range of spinel compositions in terrestrial mafic and ultramafic rocks. J Petrol 42(12):2279–2302

Bodinier JL, Dupuy C, Dostal J, Merlet C (1987) Distribution of trace transition elements in olivine and pyroxenes from ultramafic xenoliths; application of microprobe analysis. Am Mineral 72(9–10):902–913

Boudier F, Nicolas A (1995) Nature of the Moho transition zone in the Oman ophiolite. J Petrol 36(3):777–796

Brey GP, Köhler T (1990) Geothermobarometry in four-phase lherzolites II. New thermobarometers, and practical assessment of existing thermobarometers. J Petrol 31(6):1353–1378

Cipriani A, Bonatti E, Brunelli D, Ligi M (2009) 26 million years of mantle upwelling below a segment of the Mid Atlantic Ridge: the Vema Lithospheric Section revisited. Earth Planet Sci Lett 285(1–2):87–95

Coogan LA, Jenkin GRT, Wilson RN (2007) Contrasting cooling rates in the lower oceanic crust at fast- and slow-spreading ridges revealed by geospeedometry. J Petrol 48(11):1–22

Dantas C, Ceuleneer G, Gregoire M, Python M, Freydier R, Warren J, Dick HJB (2007) Pyroxenites from the Southwest Indian Ridge, 9−16°E: cumulates from incremental melt fractions produced at the top of a cold melting regime. J Petrol 48(4):646–660

Deer WA, Howie RA, Zussman J (1996) An introduction to the rock-forming minerals, 2nd edn. Prentice-Hall, London

Dennis JE Jr, Schnabel RB (1996) Numerical methods for unconstrained optimization and nonlinear equations, 16th edn. Society for Industrial and Applied Mathematics, Philadelphia

Dick HJB (1989) Abyssal peridotites, very slow spreading ridges and ocean ridge magmatism. In: Saunders AD, Norry MJ (eds) Magmatism in the Oceanic Basins, vol 42. Geological Society of London Special Publications, London, pp 71–105

Dick HJB, Bullen T (1984) Chromian spinel as a petrogenetic indicator in abyssal and alpine-type peridotites and spatially associated lavas. Contrib Mineral Petrol 86(1):54–76

Dick HJB, Fisher RL, Bryan WB (1984) Mineralogic variability of the uppermost mantle along mid-ocean ridges. Earth Planet Sci Lett 69:88–106

Dick HJB, Lin J, Schouten H (2003) An ultraslow-spreading class of ocean ridge. Nature 426(6965):405–412

Engi M (1983) Equilibria involving Al-Cr spinel: Mg-Fe exchange with olivine. Experiments, thermodynamic analysis, and consequences for geothermometry. Am J Sci 283(A):29–71

Fabriès J (1979) Spinel-olivine geothermometry in peridotites from ultramafic complexes. Contrib Mineral Petrol 69(4):329–336

Falloon TJ, Green DH, Danyushevsky LV, Faul UH (1999) Peridotite melting at 1.0 and 1.5 GPa: an experimental evaluation of techniques using diamond aggregates and mineral mixes for determination of near-solidus melts. J Petrol 40(9):1343–1375

Franz L, Seifert W, Kramer W (1997) Thermal evolution of the mantle underneath the Mid-German crystalline rise: evidence from mantle xenoliths from the Rhön area (Central Germany). Mineral Petrol 61(1):1–25

Ganguly J (2008) Thermodynamics in earth and planetary sciences. Springer, Berlin

Gasparik T, Newton RC (1984) The reversed alumina contents of orthopyroxene in equilibrium with spinel and forsterite in the system $MgO–Al_2O_3–SiO_2$. Contrib Mineral Petrol 85:186–196

Ghiorso MS, Sack RO (1995) Chemical mass transfer in magmatic processes IV. A revised and internally consistent thermodynamic model for the interpolation and extrapolation of liquid-solid equilibria in magmatic systems at elevated temperatures and pressures. Contrib Mineral Petrol 119:197–212

Harvey J, Gannoun A, Burton KW, Rogers NW, Alard O, Parkinson IJ (2006) Ancient melt extraction from the oceanic upper mantle revealed by Re-Os isotopes in abyssal peridotites from the Mid-Atlantic ridge. Earth Planet Sci Lett 244(3–4):606–621

Hellebrand E, Snow JE (2003) Deep melting and sodic metasomatism underneath the highly oblique-spreading Lena Trough (Arctic Ocean). Earth Planet Sci Lett 216(3):283–299

Hellebrand E, Snow JE, Dick HJB, Hofmann AW (2001) Coupled major and trace elements as indicators of the extent of melting in mid-ocean-ridge peridotites. Nature 410:677–681

Hellebrand E, Snow JE, Hoppe P, Hofmann AW (2002) Garnet-field melting and late-stage refertilization in 'residual' abyssal peridotites from the Central Indian Ridge. J Petrol 43(12): 2305–2338

Hellebrand E, Snow JE, Mostefaoui S, Hoppe P (2005) Trace element distribution between orthopyroxene and clinopyroxene in peridotites from the Gakkel Ridge: a SIMS and NanoSIMS study. Contrib Mineral Petrol 150(5):486–504

Hervig RL, Smith JV (1982) Temperature-dependent distribution of Cr between olivine and pyroxenes in lherzolite xenoliths. Contrib Mineral Petrol 81(3):184–189

Holland TJB, Powell R (1998) An internally consistent thermodynamic data set for phases of petrological interest. J Metamorph Geol 16(3):309–343

Ionov DA (2007) Compositional variations and heterogeneity in fertile lithospheric mantle: peridotite xenoliths in basalts from Tariat, Mongolia. Contrib Mineral Petrol 154(4):455–477

Ionov DA, Prikhodko VS, Bodinier JL, Sobolev AV, Weis D (2005) Lithospheric mantle beneath the south-eastern Siberian craton: petrology of peridotite xenoliths in basalts from the Tokinsky Stanovik. Contrib Mineral Petrol 149(6):647–665

Irvine TN (1965) Chromian spinel as a petrogenetic indicator: part 1. Theory Can J Earth Sci 2(6):648–672

Jaques AL, Green DH (1980) Anhydrous melting of peridotite at 0–15 kb pressure and the genesis of tholeiitic basalts. Contrib Mineral Petrol 73(3):287–310

Jean MM, Shervais J, Choi SH, Mukasa S (2010) Melt extraction and melt refertilization in mantle peridotite of the Coast Range ophiolite: an LA–ICP–MS study. Contrib Mineral Petrol 159(1):113–136

Johnson KTM, Dick HJB, Shimizu N (1990) Melting in the oceanic upper mantle: an ion microprobe study of diopsides in abyssal peridotites. J Geophys Res 95(B3):2661–2678

Katz RF, Spiegelman M, Langmuir CH (2003) A new parameterization of hydrous mantle melting. Geochem Geophys Geosyst 4(9):1073–1092

Kelemen PB, Shimizu N, Salters VJM (1995) Extraction of mid-ocean-ridge basalt from the upwelling mantle by focused flow of melt in dunite channels. Nature 375(6534):747–753

Kinzler RJ, Grove TL (1992) Primary magmas of mid-ocean ridge basalts 2. applications. J Geophys Res 97(B5):6907–6926

Klein EM (2003) Geochemistry of the igneous oceanic crust. In: Holland HD, Turekian KK (eds) Treatise on geochemistry, vol 3: the crust. Elsevier, Amsterdam, pp 433–463

Klein EM, Langmuir CH (1987) Global correlations of ocean ridge basalt chemistry with axial depth and crustal thickness. J Geophys Res 92(B8):8089–8115

Klemme S, O'Neill HStC (2000) The effect of Cr on the solubility of Al in orthopyroxene: experiments and thermodynamic modelling. Contrib Mineral Petrol 140(1):84–98

Liermann HP, Ganguly J (2002) Diffusion kinetics of Fe^{2+} and Mg in aluminous spinel: experimental determination and applications. Geochim Cosmochim Acta 66(16):2903–2913

Liermann HP, Ganguly J (2003) Fe^{2+}–Mg fractionation between orthopyroxene and spinel: experimental calibration in the system $FeO–MgO–Al_2O_3–Cr_2O_3–SiO_2$, and applications. Contrib Mineral Petrol 145(2):217–227

Liermann HP, Ganguly J (2007) Fe^{2+}–Mg fractionation between orthopyroxene and spinel: experimental calibration in the system $FeO–MgO–Al_2O_3–Cr_2O_3–SiO_2$, and applications. Contrib Mineral Petrol 145(4):491–491

Liu XI, O'Neill HStC (2004) The effect of Cr_2O_3 on the partial melting of spinel lherzolite in the system $CaO–MgO–Al_2O_3–SiO_2–Cr_2O_3$ at 1.1 GPa. J Petrol 45(7):1339–1368

Liu CZ, Snow JE, Hellebrand E, Brügmann G, von der Handt A, Büchl A, Hofmann AW (2008) Ancient, highly heterogeneous mantle beneath Gakkel ridge, Arctic Ocean. Nature 452(7185):311–316

Michael PJ, Bonatti E (1985) Peridotite composition from the North Atlantic: regional and tectonic variations and implications for partial melting. Earth Planet Sci Lett 73:91–104

Nagata J, Goto A, Obata M (1983) The parabolic pattern of chromium partitioning observed between pyroxenes and spinel from ultramafic rocks and its petrologic significance. Contrib Mineral Petrol 82(1):42–51

O'Neill HStC, Navrotsky A (1984) Cation distributions and thermodynamic properties of binary spinel solid solutions. Am Mineral 69(7–8):733–753

Ozawa K (1983) Evaluation of olivine-spinel geothermometry as an indicator of thermal history for peridotites. Contrib Mineral Petrol 82(1):52–65

Petric A, Jacob KT (1982) Inter- and intra-crystalline ion-exchange equilibria in the system Fe–Cr–Al–O. Solid State Ionics 6(1): 47–56

Pickering-Witter J, Johnston AD (2000) The effects of variable bulk composition on the melting systematics of fertile peridotitic assemblages. Contrib Mineral Petrol 140(2):190–211

Preß S, Witt G, Seck HA, Eonov D, Kovalenko VI (1986) Spinel peridotite xenoliths from the Tariat Depression, Mongolia. I: major element chemistry and mineralogy of a primitive mantle xenolith suite. Geochim Cosmochim Acta 50:2587–2599

Robinson JAC, Wood BJ, Blundy JD (1998) The beginning of melting of fertile and depleted peridotite at 1.5 GPa. Earth Planet Sci Lett 155(1–2):97–111

Sack RO (1982) Spinels as petrogenetic indicators: activity-composition relations at low pressures. Contrib Mineral Petrol 79:169–186

Saxena SK (1973) Thermodynamics of rock-forming crystalline solutions. Springer, Berlin

Schwab BE, Johnston A (2001) Melting systematics of modally variable, compositionally intermediate peridotites and the effects of mineral fertility. J Petrol 42(10):1789–1811

Seitz H, Altherr R, Ludwig T (1999) Partitioning of transition elements between orthopyroxene and clinopyroxene in peridotitic and websteritic xenoliths: new empirical geothermometers. Geochim Cosmochim Acta 63(23-24):3967–3982

Seyler M, Lorand JP, Dick HJB, Drouin M (2007) Pervasive melt percolation reactions in ultra-depleted refractory harzburgites at the Mid-Atlantic Ridge, 15°20′N: ODP Hole 1274A. Contrib Mineral Petrol 153(3):303–319

Stroh JM (1976) Solubility of alumina in orthopyroxene plus spinel as a geobarometer in complex systems. Applications to spinel-bearing alpine-type peridotites. Contrib Mineral Petrol 54(3): 173–188

Suzuki AM, Yasuda A, Ozawa K (2008) Cr and Al diffusion in chromite spinel: experimental determination and its implication for diffusion creep. Phys Chem Miner 35(8):433–445

Wan Z, Coogan LA, Canil D (2008) Experimental calibration of aluminum partitioning between olivine and spinel as a geothermometer. Am Mineral 93(7):1142–1147

Wasylenki LE, Baker MB, Kent A Jr, Stolper EM (2003) Near-solidus melting of the shallow upper mantle: partial melting experiments on depleted peridotite. J Petrol 44(7):1163–1191

Witt-Eickschen G, O'Neill HStC (2005) The effect of temperature on the equilibrium distribution of trace elements between clinopyroxene, orthopyroxene, olivine and spinel in upper mantle peridotite. Chem Geol 221(1–2):65–101

Witt-Eickschen G, Seck H (1991) Solubility of Ca and Al in orthopyroxene from spinel peridotite: an improved version of an empirical geothermometer. Contrib Mineral Petrol 106(4):431–439

Wolfram Research, Inc (2008) Mathematica. Version 7.0. Wolfram Research, Inc., Champaign

Workman R, Hart S (2005) Major and trace element composition of the depleted MORB mantle (DMM). Earth Planet Sci Lett 231(1–2):53–72